Control of self-collimated Bloch waves by partially flat equifrequency contours in photonic crystals

Ahyoung KimK. B. ChungJ. W. Wu

Citation: Appl. Phys. Lett. **89**, 251120 (2006); doi: 10.1063/1.2423237
View online: http://dx.doi.org/10.1063/1.2423237
View Table of Contents: http://aip.scitation.org/toc/apl/89/25
Published by the American Institute of Physics

Control of self-collimated Bloch waves by partially flat equifrequency contours in photonic crystals

Ahyoung Kim
Department of Physics, Division of Nano Sciences, Ewha Womans University, Seoul 120-750, Korea

K. B. Chung[a)]
School of Electronic and Electrical Engineering, Hongik University, Seoul 121-791, Korea

J. W. Wu
Department of Physics, Division of Nano Sciences, Ewha Womans University, Seoul 120-750, Korea

(Received 30 July 2006; accepted 17 November 2006; published online 22 December 2006)

Self-collimation effects in photonic crystals are generally investigated by employing flat equifrequency contours. Here we report, based on a partially flat equifrequency contour inducing two different group velocity vectors, the simultaneous excitation of dual self-collimated beams and the selective excitation of either of them by varying the incident angle or the width of an input Gaussian beam. With combination of the finite-difference time-domain simulation and the Fourier analysis as well as the wave vector diagram, we analyze the refractive behaviors of these self-collimated Bloch waves. © *2006 American Institute of Physics*. [DOI: 10.1063/1.2423237]

During the last few years, unusual refractive phenomena based on complex band structures in photonic crystals (PhCs), such as superprism effect,[1] negative refraction,[2–4] and self-collimation,[5,6] have attracted significant attention. Due to the ultrarefractive properties, these phenomena have been investigated for beam-steering applications and optical devices such as bends, splitters, and on-chip waveguides without defects or nonlinearities.[7–16] In particular, the self-collimation effect, which can allow a virtually diffractionless light propagation, has drawn increasing attention because of its potential for on-chip optical interconnects and nondiffractive imaging.[8–16] Generally, the self-collimation effects have been investigated by employing flat equifrequency contours (EFCs) to obtain highly self-collimated beams. However, despite intensive interests, the study on controlling self-collimated beams is still lacking. As part of the efforts, in this letter, we report that we can switch the refraction angles of self-collimated Bloch waves by utilizing partially flat EFCs inducing two different group velocity vectors, resulting in dual self-collimated beams and the selective excitation of either of them.

In our study, we consider a simple two-dimensional (2D) PhC composed of dielectric rods ($\varepsilon=12.96$) arranged on a square lattice in air. The radius of the dielectric rod is $r=0.150a$ (a is the lattice constant). Figure 1(a) shows the schematic of the employed PhC whose size is $129a\times38a$. We use an incident Gaussian beam with TE polarization (the electric field is perpendicular to the axis of the rods) and with its spatial distribution given by $\exp(-4x^2/w^2)$, where w is the $1/e$ width. The incident beam is launched into the PhC from air with an incident angle of θ_{inc} in Fig. 1(a), where the inserted dotted line indicates the normal direction to the interface. We cut the PhC normal to the ΓX direction to excite self-collimated Bloch waves in the vicinity of partial photonic band gap (PPBG).[13] We calculate the band structure by the plane wave expansion method[17] with 2601 plane waves to obtain the EFCs in Fig. 1(b). As the normalized frequency, $\omega a/2\pi c$ (c is the speed of light in vacuum), increases from 0.7100 to 0.7400, the EFCs shrink into the first Brillouin zone (1BZ) denoted by the dotted square in Fig. 1(b). Between 0.7200 and 0.7300 the PPBG along the ΓX direction disappears, and we choose the frequency of $\omega a/2\pi c=0.7255$, which shows a roughly squared shape rotated by 45° and centered at M point. To investigate the slope of the EFC precisely, we magnify a quarter of the 1BZ [the black solid square in Fig. 1(b)] in the left figure of Fig. 1(c) and insert the green solid line connecting the two X points, which

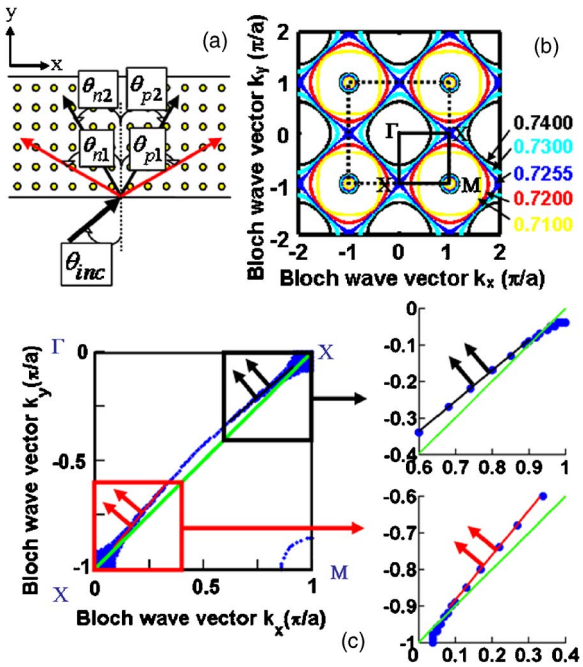

FIG. 1. (Color online) (a) Schematic of the 2D PhC. The angles are not drawn to scale. (b) The EFCs in the unit of $2\pi c/a$ in the extended zone scheme. (c) The EFC in the quarter of the 1BZ [the black solid square in (b)] is denoted by the collection of the blue dots in the left figure, in which the black and red squares are enlarged in the right, respectively. The beam with $\theta_{n1}=-50°$ ($\theta_{n2}=-40°$) is excited from the EFC within the red (black) square.

[a)]Electronic mail: kbchung@hongik.ac.kr

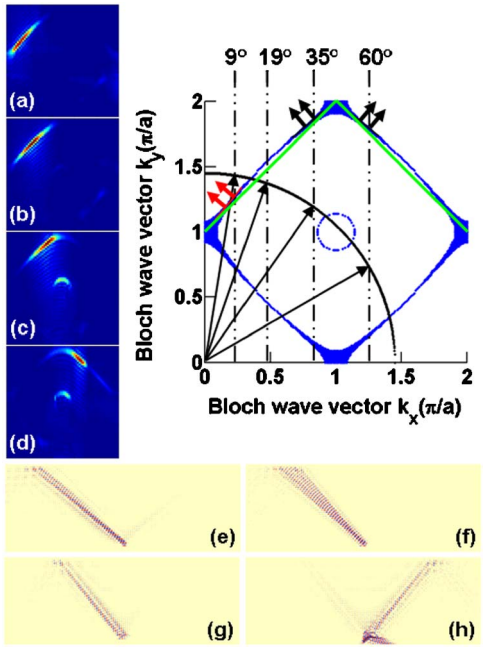

FIG. 2. (Color online) 2D Fourier transformed images [(a)–(d)] of each magnetic field distribution [(e)–(h)] for incident angles of [(a) and (e)] 9°, [(b) and (f)] 19°, [(c) and (g)] 35°, and [(d) and (h)] 60°. In (a)–(d), the red (blue) portions represent the highest (lowest) magnitude.

corresponds to a perfectly flat EFC. The shape of our calculated EFC is slightly convex in the middle rather than completely flat, but still shows two separate partially flat regions. An EFC with two separate partially flat regions (but the shape and the group velocity vector are different) is found in Ref. 16. We scale up both flat regions and show them in the right figures of Fig. 1(c), where the Bloch eigenmodes are denoted also by the blue dots, and the red and black solid lines are visual guides with the arrows indicating the direction of the group velocity vector. The eigenvalues are calculated with a more strict tolerance (less than 0.0068%) so that the blue dots are spaced. Due to two different group velocity vectors induced by the two partially flat regions, we expect dual self-collimated beams whose split angle is 10°. Additionally, due to the crystal symmetry, we expect another set of dual self-collimated beams with opposite sign of the refraction angle. We denote each refraction angle of dual self-collimated beams as $\theta_{p1}=50°$, $\theta_{p2}=40°$, $\theta_{n1}=-50°$, and $\theta_{n2}=-40°$ (the angles are described below) in Fig. 1(a), where the subscripts 1 and 2 indicate the beams excited from the EFC regions, denoted by the red and black solid squares in Fig. 1(c), respectively, and the subscripts p and n indicate the positive and negative signs of the refraction angles, respectively.

To analyze beam propagation inside the PhC, we perform the finite-difference time-domain (FDTD) simulation[18] with the perfectly-matched-layer boundary condition.[19] The magnetic field distributions for the incident angles of 9°, 19°, 35°, and 60° are shown in Figs. 2(e)–2(h), respectively. It is noted that unlike the conventional self-collimation, the refractive behaviors of our case strongly depend on the incident angle. To further confirm the analysis by the EFC and to see the Bloch mode excited by each incident beam, we perform the Fourier analysis[20] in combination with the FDTD simulation to obtain the 2D spatial-Fourier-transformed images of the magnetic fields, as shown in Figs. 2(a)–2(d). In the wave vector diagram of Fig. 2, we add an EFC for air (the black solid-line quarter circle) and the construction lines (the black dash-dot lines) for each incident angle. We employ a Gaussian beam with $w=4a$ to excite each self-collimated beam selectively. For a normal incidence (not shown), we observe simultaneously both positively and negatively refracted self-collimated beams with θ_{p1} and θ_{n1}, respectively. When θ_{inc} increases from 0° to 9°, the power of the positive beam with θ_{p1} decreases gradually, while that of the negative beam with θ_{n1} increases. At $\theta_{\text{inc}}=9°$, only the beam with θ_{n1} is dominantly excited in Fig. 2(e). For $\theta_{\text{inc}}>9°$, the negative beam with θ_{n1} starts to diverge. Its divergent behavior is maximized at $\theta_{\text{inc}}=19°$ in Fig. 2(f), when the construction line passes through the slightly convex-shaped EFC on which the two partially flat regions cross. So, the divergence angle is confined between θ_{n1} and θ_{n2}. As expected, for $\theta_{\text{inc}}>19°$ the power of the beam with θ_{n1} decreases gradually, and at $\theta_{\text{inc}}=35°$ only the beam with θ_{n2} is dominantly excited in Fig. 2(g). For $\theta_{\text{inc}}=45°$, as for the normal incidence, both positively and negatively refracted self-collimated beams with θ_{p2} and θ_{n2}, respectively, are observed (not shown) due to the change of the EFC slope. For $\theta_{\text{inc}}>45°$, the beam with θ_{n2} decreases gradually, and at $\theta_{\text{inc}}=60°$, the beam with θ_{p2} is dominantly excited in Fig. 2(h). All of the FDTD results agree well with the analysis by the wave vector diagram. Moreover, such behaviors of the self-collimated beams are clearly seen in the k-space representation[20] of each field in Figs. 2(a)–2(d). For the different incident angles of 9°, 35°, and 60°, the excited Bloch waves are localized at the partially flat regions of the EFC in Figs. 2(a), 2(c), and 2(d), respectively. For $\theta_{\text{inc}}=19°$, the Bloch wave is excited at the slightly convex EFC region in Fig. 2(b), resulting in the divergent beam in Fig. 2(f). Although there are some excitations at the small circular EFCs centered at the M points in Figs. 2(c) and 2(d), the refractive behavior is dominantly governed by the partially flat EFCs, as shown in Figs. 2(g) and 2(h). The faint components on the lower right side in Figs. 2(a) and 2(b), with opposite momentum to that of the main beam, are numerical artifacts created by small reflections at the perfectly matched layers.[21]

Next, to see the dependence on the spatial width of an incident Gaussian beam, we set the width as $w=0.4a$, $2.0a$, and $4.0a$ with a fixed $\theta_{\text{inc}}=6°$, respectively, in Figs. 3(a)–3(c). The magnetic field distributions are shown in the left of each figure. We calculate the spectral width of the beam analytically by the Fourier transform and denote it as the pink-shaded region in the right of each figure. The inserted red solid line near the center is the construction line for $\theta_{\text{inc}}=6°$, and the black dotted line is for $\theta_{\text{inc}}=0°$. In Fig. 3(a), the pink region for $w=0.4a$ is wide enough to cover the whole region of the k space, so both positively and negatively refracted dual self-collimated beams are excited simultaneously. When the spatial width increases to $w=2.0a$, the pink region narrows as in Fig. 3(b). We see that the refracted beams with θ_{p1} and θ_{n1} are excited dominantly, while the power of the beam with θ_{n2} decreases. We cannot observe the excitation of the beam with θ_{p2}, because the range of $-1<k_x<-0.5$ is outside the pink region. For $w=4.0a$ in Fig. 3(c), due to the narrow spectral width, only the negatively self-collimated Bloch wave with θ_{n1} is excited. The power of the beam with θ_{p1} decreases drastically with the beams with θ_{n2} and θ_{p2} being absent. We note that for $w>\sim 2a$, the dominant refractive behavior is determined by the beams

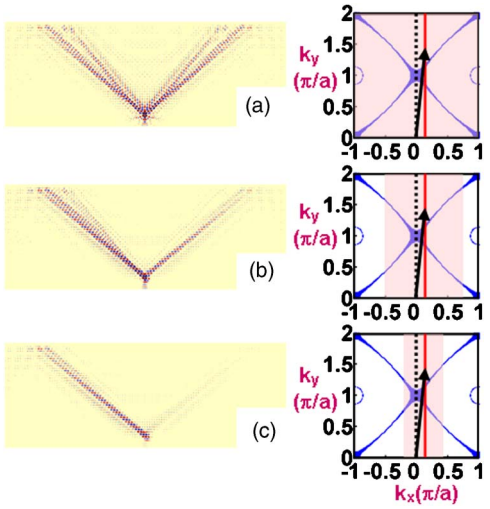

FIG. 3. (Color online) For the fixed $\theta_{inc}=6°$, the magnetic field distributions (left figures) and the wave vector diagrams (right figures) for the spatial width of an incident Gaussian beam; (a) $w=0.4a$, (b) $w=2.0a$, and (c) $w=4.0a$.

with θ_{n1} and θ_{p1}, and that for $w<\sim 2a$, the beams with θ_{n2} and θ_{p2} are additionally excited.

In this letter, by introducing a partially flat EFC, we have shown the feasibility of switching the refraction angles of self-collimated beams by varying the incident angle and the spectral width of an incident beam. Not only the selective excitation but also the simultaneous excitation of dual self-collimated beams has been observed. By combining the FDTD simulation with the Fourier analysis, we have analyzed the refractive behaviors of these self-collimated Bloch waves and found good agreements with the analysis by the wave vector diagram. We believe that this controllable self-collimation phenomena can be applied in multidirectional optical interconnects, whose channels are switchable by changing the incident angle or the width of light beam.

This work was supported by the 2006 Hongik University Research Fund, the Korea Science and Engineering Foundation through the Quantum Photonic Science Research Center at Hanyang University, and the Korea Research Foundation with Grant No. KRF 2006-005-J04001.

[1]H. Kosaka, T. Kawashima, A. Tomita, M. Notomi, T. Tamamura, T. Sato, and S. Kawakami, Phys. Rev. B **58**, R10096 (1998); Appl. Phys. Lett. **74**, 1370 (1999).
[2]M. Notomi, Phys. Rev. B **62**, 10696 (2000).
[3]C. Luo, S. G. Johnson, J. D. Joannopoulos, and J. B. Pendry, Phys. Rev. B **65**, 201104 (2002).
[4]S. Foteinopoulou and C. M. Soukoulis, Phys. Rev. B **67**, 235107 (2003).
[5]H. Kosaka, T. Kawashima, A. Tomita, M. Notomi, T. Tamamura, T. Sato, and S. Kawakami, Appl. Phys. Lett. **74**, 1212 (1999).
[6]J. Witzens, M. Loncar, and A. Scherer, IEEE J. Sel. Top. Quantum Electron. **8**, 1246 (2002).
[7]K. B. Chung and S. W. Hong, Appl. Phys. Lett. **81**, 1549 (2002).
[8]D. N. Chigrin, S. Enoch, C. M. Sotomayor Torres, and G. Tayeb, Opt. Express **11**, 1203 (2003).
[9]X. Yu and S. Fan, Appl. Phys. Lett. **83**, 3251 (2003).
[10]C. Chen, G. Jin, S. Shi, A. Sharkawy, and D. W. Prather, Appl. Phys. Lett. **84**, 3151 (2004).
[11]L. Wu, M. Mazilu, J.-F. Gallet, and T. F. Krauss, Appl. Phys. Lett. **86**, 211106 (2005).
[12]Y. Luo, W. Zhang, Y. Huang, J. Zhao, and J. Peng, Opt. Lett. **29**, 2920 (2004).
[13]Y. Peijun, C. Bo, Z. Jiangying, C. Xiyao, W. Pei1, and M. Hai1, Europhys. Lett. **70**, 197 (2005).
[14]T. Yamashita and C. J. Summers, IEEE J. Sel. Areas Commun. **23**, 1341 (2005).
[15]Z. Lu, S. Shi, J. A. Murakowski, G. J. Schneider, C. A. Schuetz, and D. W. Prather, Phys. Rev. Lett. **96**, 173902 (2006).
[16]P. T. Rakich, M. S. Dahlem, S. Tandon, M. Ibanescu, M. Soljačić, G. S. Petrich, J. D. Joannopoulos, L. A. Kolodziejski, and E. P. Ippen, Nat. Mater. **5**, 93 (2006).
[17]K. M. Ho, C. T. Chan, and C. M. Soukoulis, Phys. Rev. Lett. **65**, 3152 (1990); S. Guo and S. Albin, Opt. Express **11**, 167 (2003).
[18]K. S. Yee, IEEE Trans. Antennas Propag. **AP-14**, 302 (1966).
[19]J.-P. Berenger, J. Comput. Phys. **114**, 185 (1994).
[20]I. D. Leon and F. S. Roux, Phys. Rev. B **71**, 235105 (2005).
[21]F. S. Roux and I. D. Leon, Phys. Rev. B **74**, 113103 (2006).